Amorphous alloy/ceramic composite membrane: preparation, characterization and reaction studies

Bingsi Liu, Weilin Dai, Guohui Wu and Jing-Fa Deng*

Department of Chemistry, Fudan University, Shanghai 200433, PR China
E-mail: knfan@fudan.ihep.ac.cn

Received 25 June 1997; accepted 23 October 1997

A Ni–P amorphous alloy/ceramic membrane with high selectivity and permeability for hydrogen was prepared by a novel technique of local electroless Ni-plating with metal-activated paste. The separation factor obtained is higher for H_2/Ar compared with γ-Al_2O_3/ceramic composite membrane. In addition, two kinds of Ni–P alloy/ceramic composite membranes, as-prepared and crystallized ones, were applied to the membrane reactor of ethanol dehydrogenation, and the effect of the reaction temperature, argon sweeping rate and space time on ethanol conversion and yield of acetaldehyde was investigated. The results demonstrated that ethanol conversion in an as-prepared Ni–P amorphous alloy membrane reactor was significantly higher than that in a Ni–P alloy membrane reactor after crystallization, owing to an original structure of as-prepared Ni–P membrane. Meanwhile, the morphology of the membrane was observed by SEM. The crystallized process of non-supported Ni–P alloy membrane was detected by XRD. The surface composition and valence state of the membrane before and after reaction was investigated by XPS.

Keywords: Ni–P amorphous alloy, membrane, local electroless plating, ethanol dehydrogenation, hydrogen separation

1. Introduction

Inorganic membranes can be classified into dense and porous ones according to their pore structures. But their application in industry is generally limited, either because of extremely small permeability of dense Pd membranes or because of low separation selectivity of porous ceramic membranes. Therefore, the preparation of inorganic membranes exhibiting higher separation selectivity and higher gas permeability that are suitable for application in industry has attracted considerable research interest. As it is known, higher permeation rates can be obtained by decreasing Pd film thickness. Owing to higher hydrogen diffusion rates through the materials, alloy membranes (e.g., Pd–Ag) can also provide higher fluxes [1].

Supporting membranes on porous supports provides better mechanical strength and thermal stability than free-standing metal foils [2] and allows fabrication of membranes a few microns thick. Several synthesis techniques have been employed for the preparation of metal composites membranes, such as sputter coating [3,4], electrolytic and electroless plating [1,5,6], as well as electroless plating improved by osmosis [7–9] and the sol–gel method [10]. However, electroless plating is a technology extensively used in the preparation of Pd and Pd alloy membranes, because there is no need for considerable investments in equipment and no complex operating process. But Pd membranes are expensive, sensitive to aging and poisoning, and strongly limited by their low permeability.

Amorphous alloys possess high reactivity due to their metastable structure, high density of low coordination sites and defects, chemical homogeneity and easy reproducibility, which makes them very interesting materials in heterogeneous catalysis [11].

With regard to the study of amorphous alloys as membrane materials, only a few papers [12,13] have been reported over the past ten years. Ahmed et al. [12] prepared amorphous silicon films by ultra-low pressure chemical vapor deposition (ULPCVD). Itoh [13] et al. prepared amorphous Pd–Si alloys for hydrogen permeability and catalytic activity.

In order to improve the efficiency of hydrogen separation and permeability, we put forth a novel technique of electroless Ni-plating with metal-activated paste, by which a Ni–P amorphous alloy/ceramic composite membrane is prepared.

2. Experimental

2.1. Preparation of metal-activated paste

0.0825 g $PdCl_2$ was dissolved in 0.5 ml 1 : 1 HCl and then mixed with 14.30 ml of ethylene glycol diethyl ether to prepare a varnish, and its viscosity was adjusted with ethyl cellulose.

* To whom correspondence should be addressed.

2.2. Preparation of Ni–P amorphous alloy/ceramic composite membrane

After abrasion with sandpaper the porous ceramic tubes (o.d. 12 mm, i.d. 8 mm, average porous size 1.1–1.2 μm, porosity 0.45) were cleaned with deionized water and 0.1 M nitric acid and dried at 150°C. In order to improve the pore sizes of the substrate ceramic tubes, pre-treated ceramic tubes were dipped into SiO_2 sol (Jinshan petrochemical engineering institute, Shanghai, PR China) for 10 s, then dried at room temperature for 20 h and calcined at 700°C for 16 h. The obtained ceramic tubes were used as substrate tubes; the activated metal paste was brushed on to the outer surface of the ceramic tubes desired for electroless plating and dried at room temperature. The dried ceramic tubes were activated at 550°C. During the activation process, the organic carrier was removed and $PdCl_2$ in the top layer of the ceramic tubes was decomposed into fine metallic palladium particles. The post-treated ceramic tubes were plated in an electroless nickel bath with composition listed in table 1. After a given time, the ceramic tube with deposited Ni–P amorphous alloy membrane was washed with deionized water and dried at 80°C. The thickness of the coating was estimated by its weight and density. By this way a supported Ni–P amorphous alloy membrane on the desired outer surface of ceramic tubes was prepared.

For purpose of characterization, the Ni–P amorphous alloy membrane was deposited on smooth ceramic sheets according to the method mentioned above. After a given time, the obtained Ni–P amorphous alloy membrane was washed, dried at 80°C, and then stripped off from the smooth ceramic sheets with a scraper. By this way, the non-supported Ni–P amorphous alloy membrane was prepared.

2.3. Characterization of Ni–P amorphous alloy/ceramic composite membranes

The microstructure of the Ni–P amorphous alloy membrane was analyzed using a scanning electron microscope (SEM) (JSM-840) to determine the surface state of the membrane and substrates. The samples were sectioned into smaller pieces prior to mounting onto specimen stubs. In order to reduce specimen charging, conductive adhesive was used and the samples were sputter-coated with Au.

Table 1
Composition for electroless plating Ni solution [14]

nickel chloride	A.R.	34–45 g/ℓ
sodium citrate	A.R.	60–100 g/ℓ
triethenolamine	A.R.	70–90 ml/ℓ
ammonia chloride	A.R.	40–45 g/ℓ
sodium hypophosphite	A.R.	5–25 g/ℓ
pH	–	9–10
temperature	–	50–60°C
opening load	–	150 cm^2/ℓ

The crystallization process of the non-supported Ni–P amorphous alloy membrane was characterized by X-ray diffraction (XRD) (Regaku Dmax-γA with Cu Kα radiation). Meanwhile, the separation efficiency of the Ni–P amorphous alloy/ceramic composite membrane was evaluated by the separation factor of H_2/Ar.

The XPS experiments were carried out in a Perkin-Elmer PHI 5000C ESCA system, with a base pressure of 1×10^{-9} Torr. XPS spectra were taken using Al Kα radiation (1486.6 eV). The sample was first fixed to a sample holder and degassed in the pretreatment chamber for 2 h, then it was moved to the test chamber for XPS analysis. The charging effect of the sample was corrected by using the contaminant carbon (C 1s = 284.6 eV). Besides the Ni $2p_{3/2}$ photoelectron peaks, the spectra of P 2p are also recorded.

2.4. Ethanol dehydrogenation reaction

The reactor employed for the study was a two-tube reactor, a glass and a Ni–P alloy membrane tube as the outer and inner tube respectively, the schematic diagram of which was shown in our previous work [15]. 2 g catalyst ($Cu–P/SiO_2$, 2 wt% Cu, Cu/P = 5 mol ratio, 40–60 mesh), prepared by the ion-exchange method [16,17], was packed in the annular area between inner and outer tubes (catalyst bed height 30 mm). The ethanol was injected by a micro-feed pump, and then vaporized in the evaporator at 120°C. The ethanol vapor was carried by argon gas (50ml/min) into the membrane reactor at a W/F of 600–3800 g_{cat} min/mol, where it comes in contact with the catalyst. The hydrogen produced from the reaction permeated through the membrane into the inner tubes and was carried away by sweeping argon gas.

The reactant and products analysis was conducted by on-line gas chromatography with a conductivity detector (argon used as carrier gas, column temperature 145°C). A 4 m long Porapak P column was used to separate H_2, CO, CH_3CHO, C_2H_5OH, $C_2H_5OC_2H_5$ and $CH_3COOC_2H_5$. Because all the species could permeate through the membrane with different permeability, the products from both the outer and inner tubes were analyzed and then collected by the two cold traps separately. The weights of the condensed products were measured. The conversion, yield and selectivity are defined as follows:

$$X_{C_2H_5OH} = ([EtOH]_{in} - NC_i\%W_i - NC_o\%W_o)/[EtOH]_{in},$$

$$Y_{CH_3CHO} = (Y_i\%W_i + Y_o\%W_o)/[EtOH]_{in},$$

$$S_{CH_3CHO} = Y_{CH_3CHO}/X_{C_2H_5OH},$$

where NC_i, Y_i, W_i are non-converted ethanol, the yield of acetaldehyde and the weights of the condensed products in the inner tube respectively. NC_o, Y_o, W_o are those

in the outer tube. $[EtOH]_{in}$ is the amount of ethanol entering from an inlet through the outer path.

It is of interest to note that at the initial stage of reaction, the conversion of ethanol was obviously higher and decreased gradually with time, and reached a steady value after about 4 h. All data mentioned above were measured after 4 h.

3. Results and discussion

3.1. Crystallization process of Ni–P amorphous alloy membrane

The chemical composition of the non-supported Ni–P amorphous alloy membrane prepared by the method mentioned above, analyzed by an inductively coupled plasma (ICP) method, was found to be $Ni_{81.8}P_{18.2}$. The samples were crystallized under pure N_2 (99.99%) atmosphere at different temperatures. Figure 1 shows the X-ray diffraction (XRD) pattern of the samples at different temperatures. It was found that only a broad peak existed around 45° in the XRD pattern for the as-prepared sample. After the Ni–P amorphous alloy membrane was treated at 280°C, nickel crystal diffraction peaks appeared around $2\theta = 45°$, 37° and 52° respectively, indicating that the Ni–P amorphous alloy started to crystallize. When treatment temperature reached 450°C, the pattern is classified into two kinds of peaks, corresponding to the crystal diffraction peaks of metal Ni and Ni_3P respectively. It is of interest to note that the crystallization temperature of non-supported Ni–P amorphous alloy is obviously different from that of the supported Ni–P amorphous alloy/ceramic composite membrane [18], for which only slight crystallization was observed at 337°C due to the interaction between the clusters of deposited Ni–P amorphous alloy and the ceramic substrates.

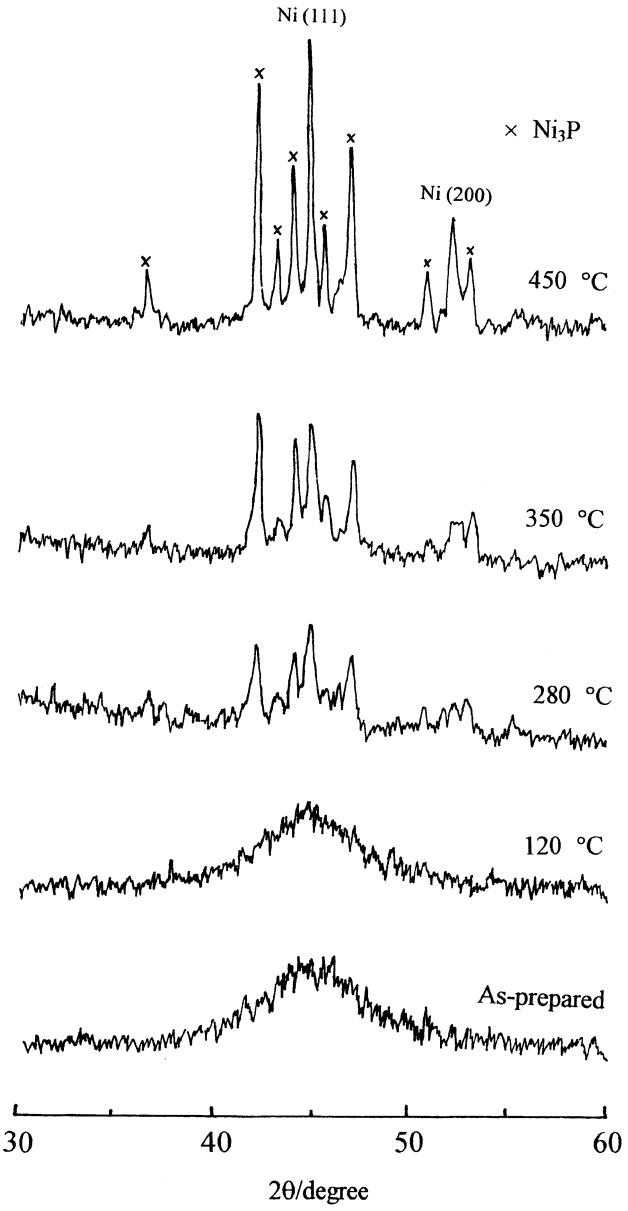

Figure 1. XRD pattern under the different conditions of crystallization for non-supported Ni–P amorphous alloy membrane.

3.2. Characterization of Ni–P amorphous alloy membrane

Figure 2 shows the microstructure of the top surface of the Ni–P amorphous alloy/ceramic composite membrane and substrate observed by scanning electron spectroscopy (SEM). The results indicate that the Ni–P amorphous particles exist in clusters uniformly deposited and that no significant crystallization and aggregation occurred on the surface of the Ni–P alloy membrane, as shown in figure 2a, whereas the pore diameters are larger for substrate ceramic tubes as shown in figure 2b. On the other hand, the XRD analysis, as shown in figure 1, indicated the existence of the amorphous structure in the as-prepared sample. The thickness of the membrane is in the range of 14–20 μm, which is similar to that estimated by weight, as previously reported [18].

The separation efficiency of the membrane is evaluated by the separation factor [19]. Figure 3 shows the effect of temperature on the separation factor ($\alpha_{H_2/Ar}$). For the γ-Al_2O_3 membrane at room temperature the separation factor, $\alpha = 4.32$, was within a limitation of the theoretical value of Knudsen diffusion ($\alpha = 4.47$), but decreased with increasing of temperature. For the Ni–P amorphous alloy/ceramic composite membrane prepared by the electroless plating technique, the separation factor for H_2/Ar remains higher than that of the γ-Al_2O_3 membrane, also exceeding the Knudsen diffusion theoretical value in the range of 400°C, and reaches maximum value at about 100°C. This means that gas diffusion through the membrane is probably related to H_2 chemisorption and surface diffusion on the wall of the

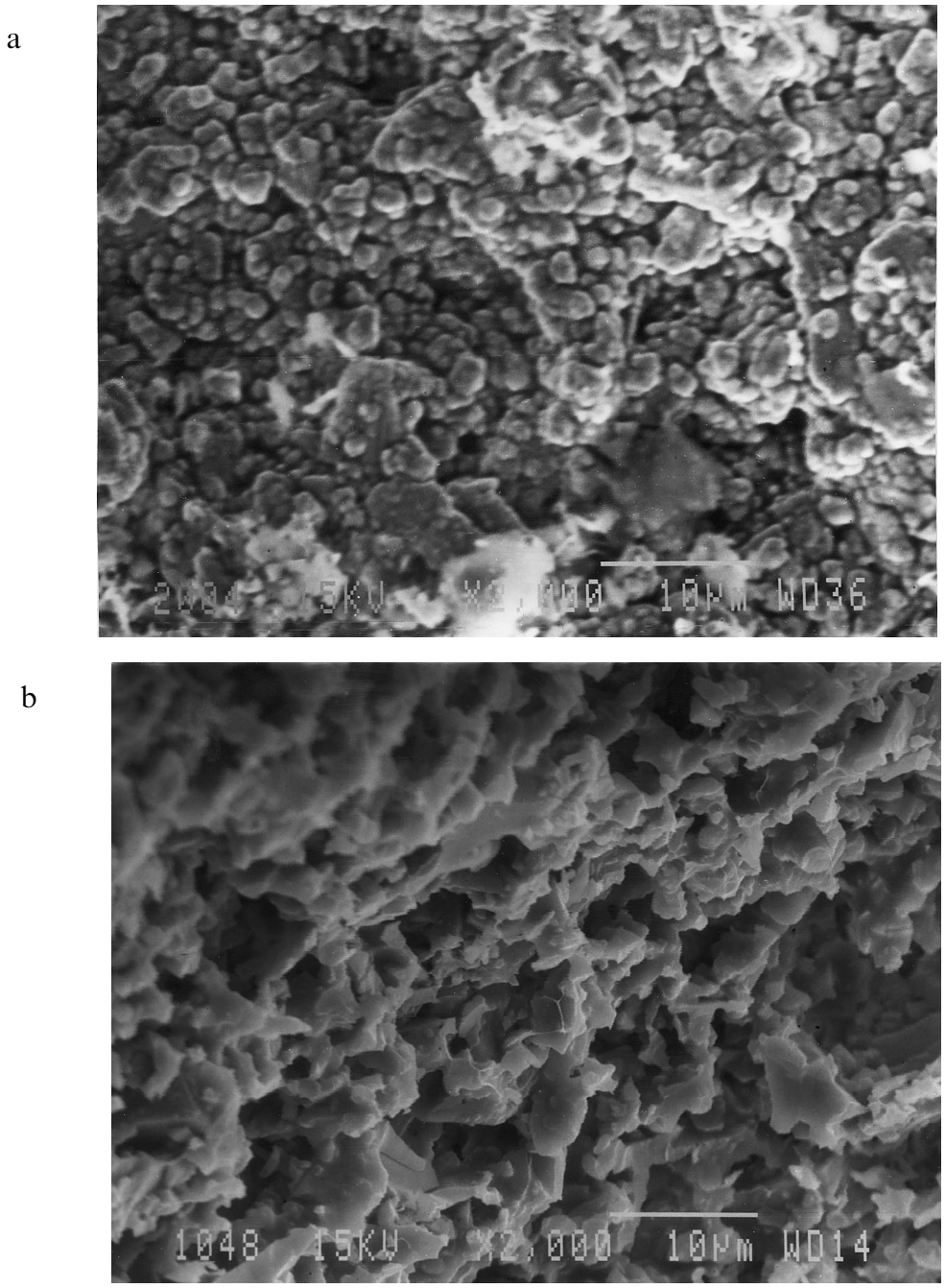

Figure 2. SEM of Ni–P amorphous alloy/ceramic composite membrane. (a) Top surface of Ni–P membrane, (b) top surface of substrates.

interstitial space, which has been proved by the experiment of hydrogen TPD [20] in a Ni–P/SiO_2 catalyst. Figure 4 shows the relationship between the pure gas permeability of H_2, He, N_2, and Ar through the Ni–P amorphous alloy membrane and the reciprocal of the square root of the molecular weight. With the exception of hydrogen, the relationship presents good linearity, which means that the permeability of Ar, N_2, and He through the membrane is mainly controlled by Knudsen diffusion, whereas the permeation rate of H_2 is higher than the extrapolation of the line mentioned above. These results further indicate that surface diffusion plays a very important part in the process of hydrogen permeation through the membrane, but with the increase of temperature, the separation factor of H_2/Ar declined owing to the diffusion of phosphorus from the bulk to the surface, as discussed in the following.

3.3. Ethanol dehydrogenation reaction

For the sake of comparison, the equilibrium yields of acetaldehyde at different temperatures and a given pressure were calculated by means of thermodynamic data [21], as shown in figure 5b.

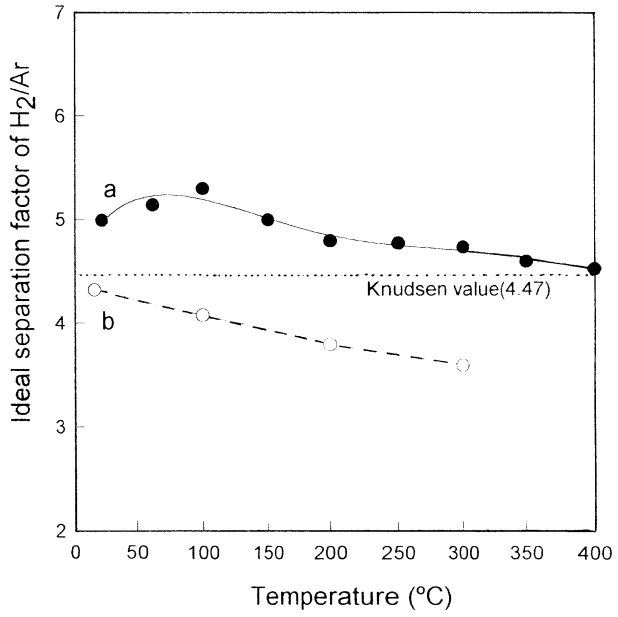

Figure 3. The separation factor for H_2/Ar vs. temperature. (a) Ni–P amorphous alloy/ceramic composite membrane, (b) γ-Al_2O_3/ceramic composite membrane.

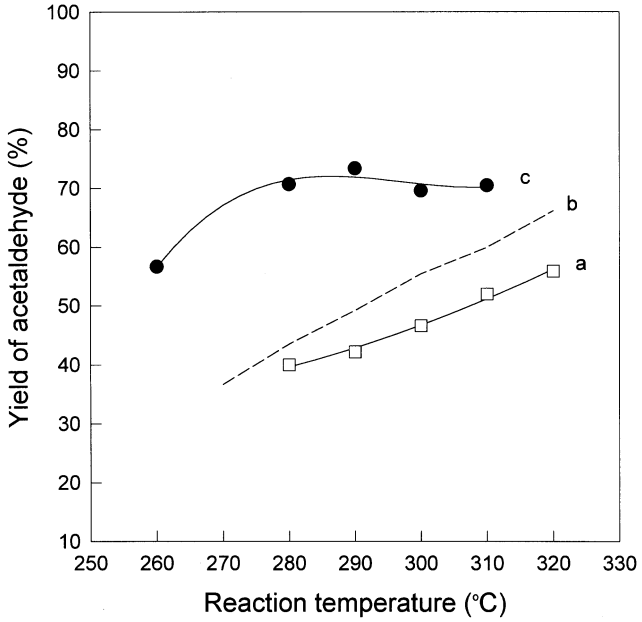

Figure 5. The yield of acetaldehyde vs. reaction temperature. (a) Conventional reactor, (b) equilibrium value, (c) as-prepared Ni–P amorphous alloy membrane reactor. Ar sweeping rate: 40 ml/min, W/F: 1468.6 g_{cat} min mol^{-1}.

The ethanol dehydrogenation reaction was conducted in a Ni–P amorphous alloy/ceramic composite membrane reactor with simultaneous separation of hydrogen. Prior to reaction, the catalyst was reduced in flowing hydrogen at 350°C for 2.5 h. Figure 5 shows the yields of acetaldehyde in the conventional reactor, the Ni–P amorphous alloy/ceramic composite membrane reactor, and thermodynamic equilibrium yield of acetaldehyde related to the reaction temperature. As shown in figure 5, the yield of acetaldehyde in the Ni–P amorphous alloy/ceramic composite membrane reactor is higher than that in the conventional reactor and obviously exceeds the thermodynamic equilibrium value. This is because hydrogen produced from the reaction diffused to the other side of the Ni–P amorphous alloy/ceramic composite membrane and was carried

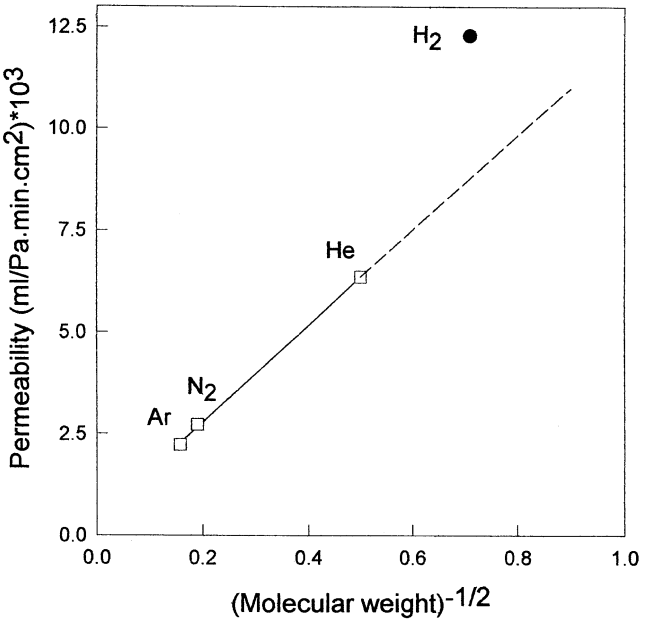

Figure 4. Permeability of H_2, N_2, Ar and He through Ni–P amorphous alloy/ceramic composite membrane at 100°C.

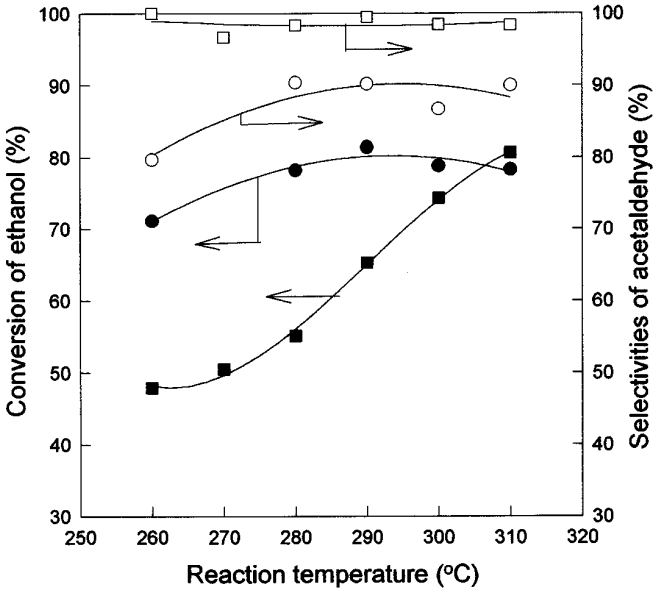

Figure 6. Ethanol conversion and selectivity of acetaldehyde vs. reaction temperature. (●, ○) As-prepared Ni–P membrane reactor, (■, □) Ni–P membrane reactor after crystallization. Ar sweeping rate: 40 ml/min, W/F: 1512.4 g_{cat} min mol^{-1}.

away by flowing argon, thereby positively shifting the chemical equilibrium.

Figure 6 shows that the ethanol conversion and the selectivity to acetaldehyde change with reaction temperature. For a given space time ($W/F = 1512.4$ g_{cat} min mol^{-1}, where W (g) is the weight of the catalyst and F (mol/min) is the feed rate), at the beginning, the ethanol conversion in the as-prepared Ni–P amorphous alloy/ceramic composite membrane reactor is obviously higher than that in the Ni–P alloy/ceramic composite membrane reactor after crystallization. This is because the Ni–P amorphous alloy possesses an original structure of metastable "cluster", a low coordination site and defects, as well as interstitial space available for hydrogen diffusion. These properties promote the permselectivity of hydrogen through the membrane, enhancing the conversion of ethanol. But with the increase of reaction temperature the ethanol conversions in the two kinds of membrane reactors gradually tend to be identical due to gradual crystallization of Ni–P amorphous alloy. This has been proved by investigating the crystallization process of non-supported Ni–P amorphous alloy membrane.

The efficiency of the membrane reactor depends on the permeability of hydrogen, which is partly related to the flow rate of the sweeping gas. Figure 7 shows the relationship between ethanol conversion and the flow rate of argon sweeping in two Ni–P alloy membrane reactors, as-prepared and crystallized ones. But it is of interest to note that for the as-prepared Ni–P amorphous alloy membrane reactor, ethanol conversion increased slowly and then gradually declined with increase of Ar sweeping speed. We may speculate that the as-prepared Ni–P amorphous alloy membrane not only selectively permeated hydrogen but also partly permeated ethanol. Therefore, when the rate of permeated gas exceeds the reaction rate of ethanol dehydrogenation, increase of Ar sweeping rate is disadvantageous to reaction.

The effect of the feed rate of ethanol on its conversion and the selectivity to acetaldehyde is shown in figure 8. The results demonstrate that the ethanol conversion and the selectivity to acetaldehyde increased with increasing space time because of the increase of the contact time of the reactant with the catalyst.

For comparison, a blank test was performed in the Ni–P amorphous alloy/ceramic membrane reactor without catalyst but under the same operating conditions. The catalyst was displaced by quartz sand to keep the same flow resistance as in the membrane reactor with catalyst. The results demonstrated that the yields of acetaldehyde were less than 3% in general and the maximum value obtained at 290°C was 5.7%. Therefore, the catalyst activity of Ni–P amorphous alloy membrane itself is negligible.

3.4. XPS investigation of Ni–P amorphous alloy/ceramic composite membrane before and after reaction

The XPS spectra of the as-prepared $Ni_{81.8}P_{18.2}$ amorphous alloy membrane are shown in figures 9 and 10. In figure 9, curves a and c show the XPS spectra of Ni $2p_{3/2}$ before and after reaction, while curves b and d correspond to the states after a 5 min Ar^+ sputtering of states a and c, respectively (only Ni $2p_{3/2}$ sub-bands are considered instead of the Ni $2p_{1/2}$ sub-bands [22,23], because

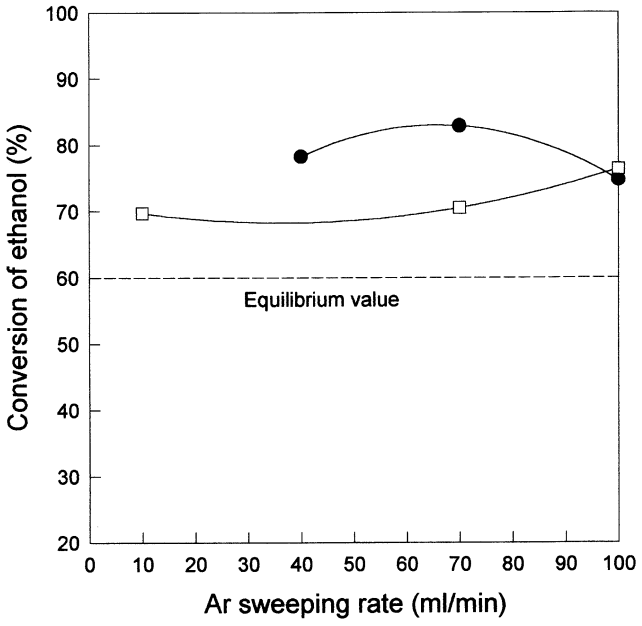

Figure 7. The effect of the Ar sweeping rate on ethanol conversion in Ni–P alloy membrane reactor before and after crystallization. (●) Before crystallization, (□) after crystallization. Reaction temperature: 310°C, W/F: 1468.6 g_{cat} min mol^{-1}.

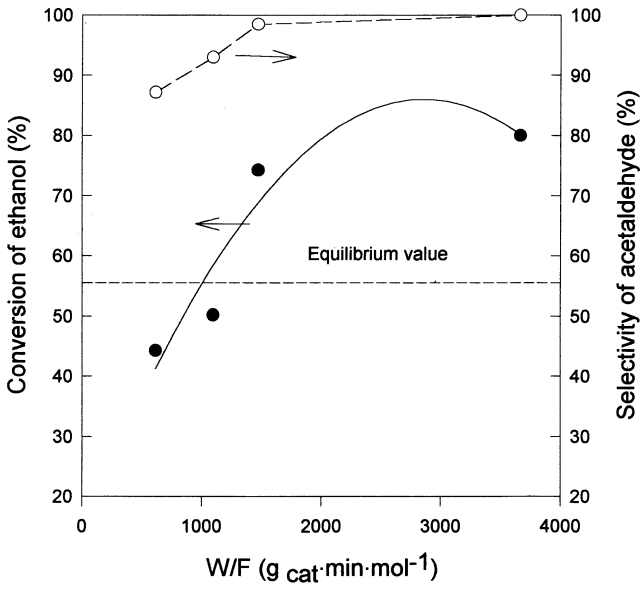

Figure 8. The effect of space time, W/F, on the ethanol conversion. Reaction temperature: 300°C, rate of Ar sweeping: 50 ml/min.

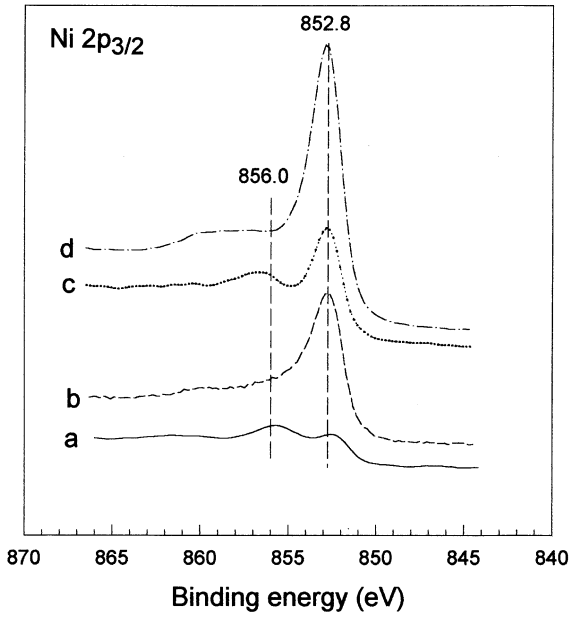

Figure 9. XPS spectra of nickel in Ni–P amorphous alloy/ceramic composite membrane. (a) Before reaction, (b) Ar^+ sputtering for 5 min. (c) After reaction, (d) Ar^+ sputtering for 5 min.

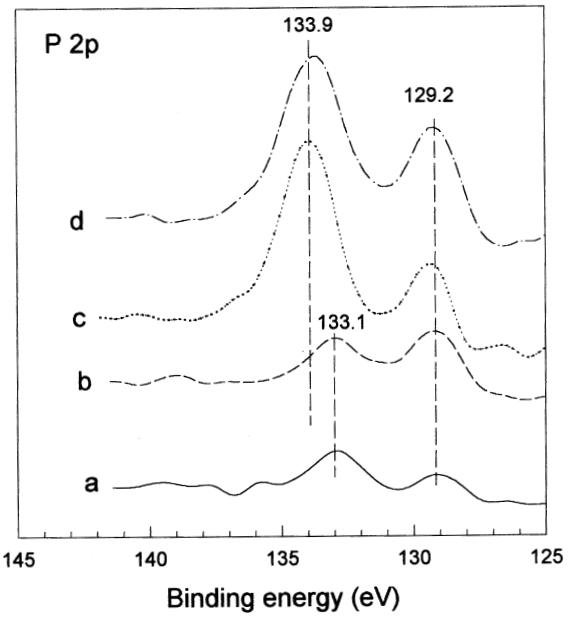

Figure 10. XPS spectra of phosphorus in Ni–P amorphous alloy/ceramic composite membrane (the surface treatment is the same as in figure 9).

the former have a much better signal to noise ratio and can supply the same information as the latter). It is obvious that all the four spectra contain the elemental Ni $2p_{3/2}$ peak at 852.8 eV close to the value previously reported [24]. It is easy to find the difference between the Ni $2p_{3/2}$ peak before and after reaction. Although elemental Ni and Ni_2O_3 are all present, which can be confirmed by the high-energy shoulders on the metallic Ni line at energies of about 856.0 eV, the relative contents of the oxidized state and the elemental state are totally different. The elemental one increases after reaction. This result reveals that the reaction mixture can partially reduce the oxidized film on the surface of the membrane. From the two curves after Ar^+ sputtering, except for the metallic Ni, no other chemical states of nickel can be found, which illustrates that the oxidized film may result from the oxidation of Ni–P amorphous alloy surface and can be removed by Ar^+ sputtering because of its thinness.

Also, the XPS spectra of P 2p corresponding to the four states as mentioned above are shown in figure 10, which demonstrates the presence of the oxidation (P^{5+}) and elemental state of phosphorus (P^0). The XPS peaks at 129.2 eV can be ascribed to the amorphous elemental P from the amorphous alloy membrane, while the peaks at 133.1 eV (before reaction) or 133.9 eV (after reaction) can be assigned to phosphates (HPO_4^{2-} and $H_2PO_4^-$) [25]. As mentioned in the experimental section, H_2 is present in the reaction mixture and can reduce oxidized nickel producing H^+ and elemental nickel. Then H^+ will combine with HPO_4^{2-} to form $H_2PO_4^-$. Similar results were obtained by Chen et al. [26] by exposing Ni–P amorphous alloy to hydrogen at 553 K.

According to the positions of the Ni $2p_{3/2}$ and P 2p XPS peaks, we find that, in the Ni–P amorphous alloy membrane, Ni $2p_{3/2}$ peaks shifted positively by 0.6 eV compared with pure nickel (852.2 eV) as reported previously [27], while P 2p XPS peaks shifted negatively by 0.8 eV as comparison to red phosphorus (130.0 eV) [28]. This result indicates that there is an interaction between Ni and P with charge transfer from Ni to P.

Table 2 shows the bulk and surface composition in the Ni–P amorphous alloy membrane at different states by using ICP and relative XPS analysis. From table 2, we can find that the surface is enriched by P either before or after reaction. On the other hand, the surface content of P is much greater after reaction (from 24.0 to 34.3%), indicating the diffusion of phosphorus from the bulk to the surface after reaction. If the top surface is removed

Table 2
The composition of Ni–P amorphous alloy [a]

	ICP	(a)	(b)	(c)	(d)
Composition	$Ni_{81.8}P_{18.2}$	$Ni_{76}P_{24}$	$Ni_{83.2}P_{16.8}$	$Ni_{65.7}P_{34.3}$	$Ni_{83.2}P_{16.8}$

[a] (a) Before reaction; (b) 5 min Ar^+ sputtering of a; (c) after reaction; (d) 5 min Ar^+ sputtering of (c).

by Ar^+ sputtering, the chemical composition of the fresh surface is very similar to the bulk. That means that the chemical composition on the top surface ($\sim$ 4 nm) is different from that of the bulk.

4. Conclusions

The Ni–P amorphous alloy/ceramic composite membrane with high selectivity and permeability for hydrogen was prepared by a novel technique of local electroless plating. The separation factor for H_2/Ar through the membrane was measured, indicating that it was obviously higher than that through a porous inorganic one.

Two kinds of Ni–P alloy/ceramic composite membranes, as-prepared and crystallized ones, were applied to the membrane reactor of ethanol dehydrogenation, indicating that the former presents higher ethanol conversion than the latter.

XPS results indicate (1) interaction between Ni and P with charge transfer from Ni to P on the surface of the Ni–P alloy membrane and (2) diffusion of phosphorus from the bulk to the surface before and after reaction.

Acknowledgement

We gratefully acknowledge financial support from National Natural Science Foundation of China and Sinopec.

References

[1] S. Uemiya, T. Matsuda and E. Kikuchi, J. Membrane Sci. 56 (1991) 315.
[2] V.M. Gryaznov, Z. Physik. Chemie NF 147 (1986) 123.
[3] V.M. Gryaznov, O.S. Serebryannikova, M.Yu. Serov, M.M. Ermilova, A.N. Karavanov, A.P. Mischenko and N.V. Orekhova, Appl. Catal. A 96 (1993) 15.
[4] M. Konno, M. Shindo, S. Sugawara and S. Saito, J. Membrane Sci. 37 (1988) 193.
[5] J.P. Collins and J.D. Way, Ind. Eng. Chem. Res. 32 (1993) 3006.
[6] S. Uemiya, I. Koike and E. Kikuchi, Appl. Catal. A 76 (1991) 171.
[7] K.L. Yeung, R. Aravind, R.J.X. Zawada, J. Szegner, G. Cao and A. Varma, Chem. Eng. Sci. 49 (1994) 4823.
[8] K.L. Yeung and A. Varma, AIChE J. 41 (1995) 2131.
[9] K.L. Yeung, J.M. Sebastian and A. Varma, Catal. Today 25 (1995) 231.
[10] A. Li, G. Xiong, J. Gu and L. Zheng, J. Membrane Sci. 110 (1996) 257.
[11] M. Stancheva, S. Manev, D. Lazarov and M. Mitov, Appl. Catal. A 135 (1996) L19.
[12] W. Ahmed, D.B. Meakin, J. Stoemenos, N.A. Economou and R.D. Pilkington, J. Mater. Sci. 27 (1992) 479.
[13] N. Itoh, T. Machida, W.C. Xu, H. Kimura and T. Masumoto, Catal. Today 25 (1995) 241.
[14] B. Liu, W. Yuan and Q. Liu, Mater. Protection 26(3) (1993) 23.
[15] B. Liu, Y. Cao and J. Deng, Separation Sci. Technol., in press.
[16] T. Sodesawa, M. Nagacho, A. Onodera and F. Nozaki, J. Catal. 102 (1986) 460.
[17] T. Yamamoto, A. Shimoda, T. Okuhara and M. Misono, Chem. Lett. (1988) 273.
[18] B. Liu, H. Li, Y. Cao, J. Deng, C. Sheng and S. Zhou, J. Membrane Sci., in press.
[19] J. Deng, Z. Cao and B. Zhou, Appl. Catal. A 132 (1995) 9.
[20] J. Deng and X. Zhang, Solid State Ionics 32/33 (1989) 1006.
[21] J. Deng and K. Fan, *Physical Chemistry* (Higher Education Press, Shanghai, 1995).
[22] J. Grimblot, J.P. Bonnelle and J.P. Beaufils, J. Electron Spectrosc. Relat. Phenom. 8 (1976) 437.
[23] G. Tyuliev and S. Angelov, Appl. Surf. Sci. 32 (1988) 381.
[24] S. Yoshida, H. Yamashita, T. Funabiki and T. Yonezawa, J. Chem. Soc. Faraday Trans. I 80 (1984) 1435.
[25] P. Swift, Surf. Interface Anal. 4 (1982) 47.
[26] J. Deng, H. Chen, X. Bao and M. Muhler, Appl. Surf. Sci. 81 (1994) 341.
[27] V.V. Nemoshkalenko, A.I. Kharlamov, T.I. Serebryakova and V.G. Aleshin, Kinet. Catal. 19 (1978) 1567.
[28] M. Schaerli and J.Z. Brunner, J. Phys. B 42 (1981) 485.